

^{17}O NMR Gives Unprecedented Insights into the Structure of Supported Catalysts and Their Interaction with the Silica Carrier

Nicolas Merle,[†] Julien Trébosc,[‡] Anne Baudouin,[†] Iker Del Rosal,[§] Laurent Maron,^{*,§} Kai Szeto,[†] Marie Genelot,[‡] André Mortreux,[‡] Mostafa Taoufik,^{*,†} Laurent Delevoye,^{*,‡} and Régis M. Gauvin^{*,‡}

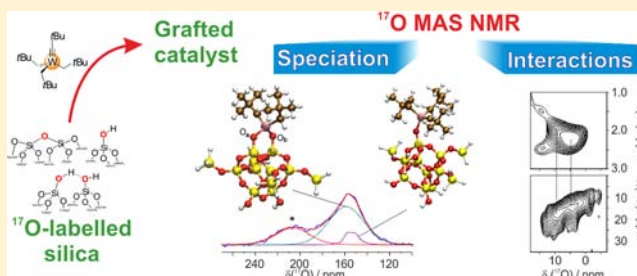
[†]Laboratoire de Chimie Organométallique de Surface (C2P2-UMR 5265 CNRS/UCBL/ICL) ESCPE Lyon, 43 Boulevard du 11 Novembre 1918, F-69616 Villeurbanne Cedex, France

[‡]Université Lille Nord de France, CNRS UMR8181, Unité de Catalyse et de Chimie du Solide, UCCS USTL, F-59655 Villeneuve d'Ascq, France

[§]Université de Toulouse, INSA, UPS, CNRS-UMR5215, LPCNO, 135 avenue de Rangueil, 31077 Toulouse, France

S Supporting Information

ABSTRACT: Flame silica was surface-labeled with ^{17}O , through isotopic enrichment of both siloxanes and silanols. After heat treatment at 200 and 700 °C under vacuum, the resulting partially dehydroxylated silica materials were investigated by high-field solid-state ^1H and ^{17}O NMR. More specifically, MQ MAS and HMQC sequences were used to probe the ^{17}O local environment. In a further step, these ^{17}O -tagged supports were used for the preparation of supported catalysts by reaction with perhydrocarbyl transition metal derivatives (zirconium tetraalkyl, tantalum trisalkyl-alkylidene, and tungsten trisalkyl-alkylidyne complexes). Detailed ^{17}O 1D and 2D MQ and HMQC MAS NMR studies demonstrate that signals in the Si–OH, Si–O–Si, and Si–O–metal regions are highly sensitive to local structural modifications, thanks to ^{17}O wide chemical shift and quadrupolar constant ranges. Experimental results were supported by DFT calculations. From the selective surface labeling, unprecedented information on interactions between supported catalysts and their inorganic carrier has been extracted.



INTRODUCTION

Heterogeneous catalysis holds a key position in the world chemical industry. A fair share of it implies transition metal containing materials, in which a metallic component is immobilized onto an inorganic carrier. Most often, development and discoveries are highly empirical, and heterogeneous catalysts present different types of active (and nonactive) surface sites.¹ Understanding of their molecular structure is of prime importance, as this could pave the way to enhanced preparation methods and better understanding of key phases of a catalyst life (initiation, operation, and deactivation). In all these aspects, doubtlessly, the study of the interaction between a metal center (M) and its inorganic carrier ($\text{M}'_x\text{O}_y$) is of crucial importance.

The characterization of surface species can be achieved with the help of various techniques.² For instance, X-ray absorption spectroscopy allows access to information on heavy nuclei, namely metal centers, indicating the nature and number of ligands surrounding the metal within its first (and, with lesser accuracy, second) coordination sphere. Vibrational spectroscopies, such as infrared and Raman, are unrivaled when probing the presence of specific groups in a given material, and they proved to be highly sensitive to detect subtle changes at the molecular level. If metal–support M–O–M' bands are

observed, their interpretation is sometimes controversial and does not provide accurate structural information.

However, a technique of choice for the study of immobilized inorganic or organometallic centers is solid-state MAS NMR, which emerged over the recent years as a most versatile tool for the analysis of materials down to the molecular level.³ The vast number of NMR active nuclei allows for deep studies to be carried out. These involve the recording not only of simple monodimensional spectra but also of bidimensional homo- and heteronuclear correlation spectra. In this latter case, one can gather precious information, such as spatial proximity or connectivity between given nuclei. If the most commonly reported studies involve the nuclei featuring a nuclear spin value (*S*) of $1/2$, such as ^1H and ^{13}C ,⁴ elements of other *S* can also yield informative NMR data. Indeed, some key elements are well suited for NMR studies, such as ^{27}Al , ^{51}V , or ^{93}Nb , for instance. As most of them are quadrupolar nuclei, enhanced resolution and sensitivity are obtained by combining very high field and multiple quantum (MQ-MAS) 2D spectral acquisition.⁵ However, the metal center may in some instance be NMR silent, or notoriously difficult to detect, or simply give

Received: February 2, 2012

Published: May 9, 2012

rise to uninformative data. It is therefore of interest to come up with a new approach of the widest applicability for the NMR studies on transition-metal-based catalysts immobilized on inorganic carriers.

The common point between all of the systems, which involve transition-metal species grafted onto inorganic oxide support (M'_xO_y), is the involvement of one or several $M-O-M'$ fragments. Furthermore, the bridging oxygen atoms from the support ($M'-O-M'$) may also interact by coordination to the metal center. Another major issue is the determination of the spatial proximities of the various fragments of the catalytic system: the assessment of the relative configuration of supported fragments and of inorganic carriers functionalities (hydroxyls or $M'OM'$) would be of high mechanistic and structural interest, affording information at the molecular level.

Considering these points, we envisioned to use ^{17}O labeled inorganic supports as a new tool to study supported catalysts. ^{17}O solid-state MAS NMR is nowadays increasingly accessible, and it yielded fruitful information on the characterization of inorganic materials.⁶ Some of these studies involve catalysis-related oxides.⁷ In most cases, the ^{17}O MAS NMR approach benefits not only from the wide chemical shift (CS) range but also from high sensitivity of the quadrupolar coupling constant (C_Q) to the local environment. As this approach is novel and may prove a difficult task, special care must be paid to the design of the methodology. Indeed, to successfully tackle this problem, one must address several points:

(1) To select an inorganic support of well understood structure and reactivity. In this case, amorphous silica is a very widely used support in catalyst preparations, which presents a well-established chemistry;⁸ its surface comprises $Si-O-Si$ and $SiOH$ moieties, with various configurations. Indeed, siloxanes can be part of polysiloxane rings of varying sizes, whereas several types of silanols are known, depending on the surface density. These structural types are dependent on the support dehydroxylation temperature, which in turn impacts on the silica's reactivity with incoming transition metal reagents.

(2) To successfully label the support's surface without significant incorporation of ^{17}O nuclei in the bulk in order not to blur the surface-related information. ^{17}O labeled siliceous materials have already been described in the literature. These were prepared via sol-gel methodology, using labeled water and silicate network formers,⁹ or by high temperature reaction with dioxygen.¹⁰ These procedures lead to materials with ^{17}O centers diluted throughout the material, namely in the bulk and on the surface. However, as we wanted to focus on surface chemistry, we needed an approach that would afford selective labeling of the surface oxygen ($SiOSi$ or $SiOH$) and give the minimum possible signal for the bulk $SiOSi$.

(3) To use the most selective preparation methodology to immobilize transition metal centers. In this aspect, surface organometallic chemistry (SOMC) enables the preparation of catalysts of well-defined structure through grafting of organometallic fragments onto inorganic supports.¹¹ Numerous organometallic silica surface species have been prepared and fully characterized as well-defined species. From this library of examples, selected families of species can be used to refine the level of understanding for the interaction of the grafted organometallics with the support, as sought through the use of ^{17}O MAS NMR.

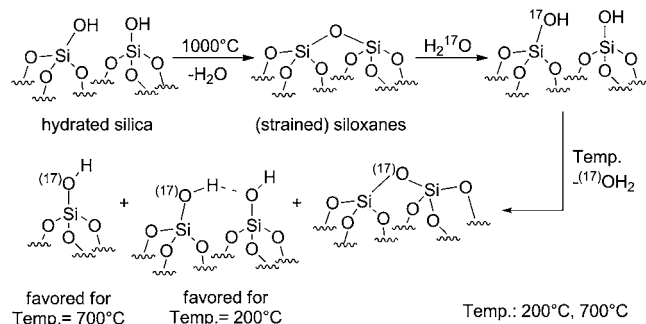
In the present contribution, we will show that this strategy is successful and provides unprecedented information on the catalyst-support interaction. This was accomplished through

^{17}O MAS NMR characterization of the different oxygen environment by scrutinizing CS and C_Q modifications, using the most advanced correlation methods combined with DFT calculations.

RESULTS

1. ^{17}O -Surface Labeled Silica Preparation and Characterization. The chosen silica is Aerosil 200, a nonporous flame silica from Evonik featuring a specific area of $200 \text{ m}^2 \cdot \text{g}^{-1}$. After calcination, it was rehydrated using ^{17}O -labeled water (70%) and subjected to thermal treatment at 200 and 700 °C under vacuum, to afford SiO_2^{*-200} and SiO_2^{*-700} , respectively. In this case, our procedure differs from reported exchange reactions with $^{17}OH_2$ in that the annealing generates highly strained surface siloxanes which react with enriched water to regenerate silanols (Scheme 1).¹² The ensuing thermal treatment affords the targeted silanol population and also generates labeled siloxanes from condensation involving labeled silanol(s) (*vide infra*).

Scheme 1. Enrichment Procedure and Schematic Reactivity



As extensively documented, the silanol population is affected by this treatment: as SiO_2^{*-200} features vicinal, geminal, and "isolated" (non-interacting) silanols, SiO_2^{*-700} only bears the latter type of silanol groups.⁸ This transcribes into both infrared and 1H MAS NMR spectra of these materials (Figure 1).

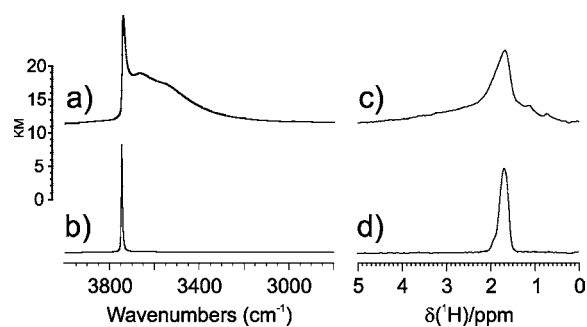


Figure 1. DRIFTS (a and b) and 1H MAS NMR spectra (c and d, 18.8 T) of SiO_2^{*-200} and SiO_2^{*-700} , respectively.

SiO_2^{*-700} gives rise to spectroscopic features indicative of a narrow distribution (a 3747 cm^{-1} peak for ν_{OH} in the IR infrared spectrum, and a sharp signal at 1.7 ppm in the 1H NMR spectrum; Figure 1). On the other hand, the IR spectrum of SiO_2^{*-200} comprises peaks for non-interacting (sharp, 3747 cm^{-1}) and vicinal, H-bonded $SiOH$ groups (broad, with maxima at 3660 and 3570 cm^{-1}). The latter are indicative of strong H-bonding interactions. Accordingly, the 1H NMR

spectrum features two signals, namely a sharp, asymmetric contribution at 1.75 ppm (non-interacting silanols) and a broader one spanning from 4 to 1 ppm (H-bonded vicinal silanols). Note that the lack of resolution prevents further assignment regarding geminal and isolated silanols. The former are described as not being involved in hydrogen-bonding,¹³ and their signal may be comprised in the sharper component (peak at 1.75 ppm). These elements are in line with previous results on ¹H NMR studies on flame silica treated at various temperatures, with the most noteworthy being those by Maciel and co-workers.¹⁴ The use of high magnetic field does not induce any increase in resolution.

¹⁷O MAS NMR of SiO₂*₋₂₀₀ and SiO₂*₋₇₀₀ display signals in the Si–O–Si and Si–OH regions (50–10 ppm and 10 to –20 ppm, respectively), as previously described (Figure 2).¹⁵ We

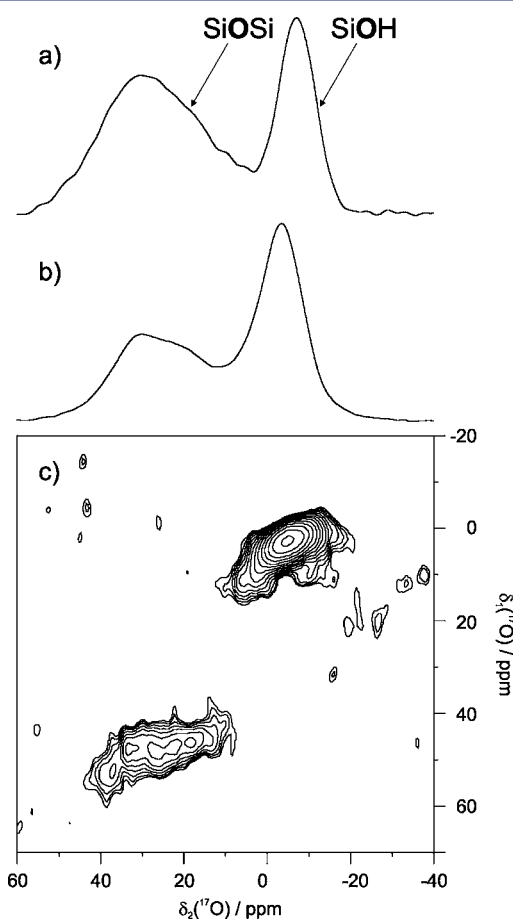


Figure 2. ¹⁷O MAS NMR spectra at 18.8 T of (a) SiO₂*₋₇₀₀ (number of scans ns = 38880, recycling delay rd = 1 s, MAS rate = 20 kHz) and (b) SiO₂*₋₂₀₀ (ns = 40960, rd = 1 s, MAS rate = 20 kHz), and (c) MQ MAS NMR spectrum of SiO₂*₋₂₀₀ (ns = 12000, rd = 1 s, time domain t₁ = 30, MAS rate = 15 kHz, acquisition time = 100 h).

checked that nonenriched SiO₂-200 does not give rise to any of these signals under similar experimental conditions. A closer look between the ¹⁷O MAS NMR spectra of SiO₂*₋₂₀₀ and SiO₂*₋₇₀₀ reveals slightly distinct features: (1) the ratio Si–O–Si vs Si–OH increases with the annealing temperature, in line with the well-established condensation mechanism occurring during annealing; (2) the silanol chemical shift decreases from –4.2 to –7.4 ppm when going from SiO₂*₋₂₀₀ to SiO₂*₋₇₀₀; (3) the width of the Si–O–Si pattern increases when going from

SiO₂*₋₂₀₀ to SiO₂*₋₇₀₀. The latter feature indicates emergence of further contributions in the signal.

To investigate selectively the silanol region, we resorted to J-HMQC,¹⁶ which filters the signal by selecting only the nuclei featuring scalar (*J*) coupling. Indeed, the ¹H–¹⁷O J-HMQC spectra of SiO₂*₋₂₀₀ and SiO₂*₋₇₀₀ present the SiOH signals as a single contribution (Figure 3). The simplest spectrum is that of

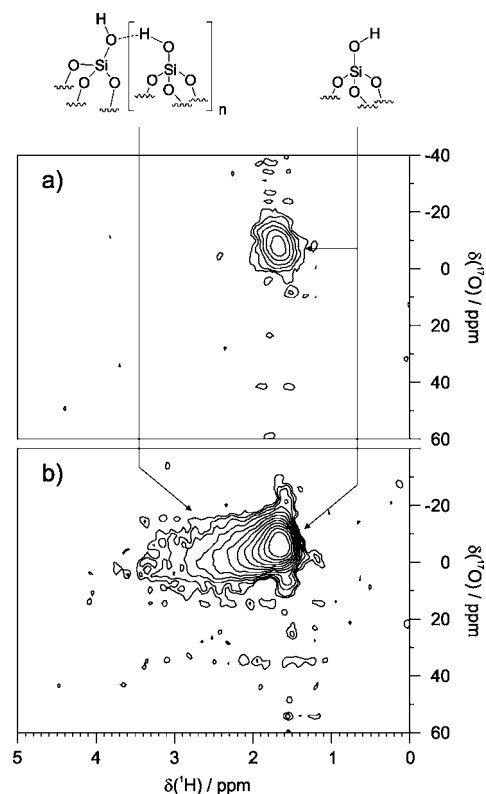


Figure 3. ¹H–¹⁷O J-HMQC MAS NMR spectra at 18.8 T of (a) SiO₂*₋₇₀₀ and (b) SiO₂*₋₂₀₀ (ns = 64, rd = 5 s, t₁ = 80, MAS rate = 19 kHz, acquisition time = 7 h).

SiO₂*₋₇₀₀, as non-interacting silanols are the only hydroxyl group type present in the material. A sharp correlation associates the ¹H and ¹⁷O signals at 1.8 and –7.4 ppm, respectively. On the other hand, the SiO₂*₋₂₀₀ spectrum presents a similar correlation at 1.6 ppm/–5.8 ppm (¹H/¹⁷O), accounting for non- or weakly interacting silanols, along with a large contribution spanning from 3.5 to 1.5 ppm and 10 to –20 ppm in ¹H and ¹⁷O dimensions, respectively. This last one originates from the strongly interacting protons (H-bonded silanols, seen here as clusters). The scalar coupling constant ¹J_{OH} for the signal of the non-interacting silanols was determined by fitting the build-up curve of the J-HMQC signal, affording a value of 107 Hz (Figure S2 in the Supporting Information).

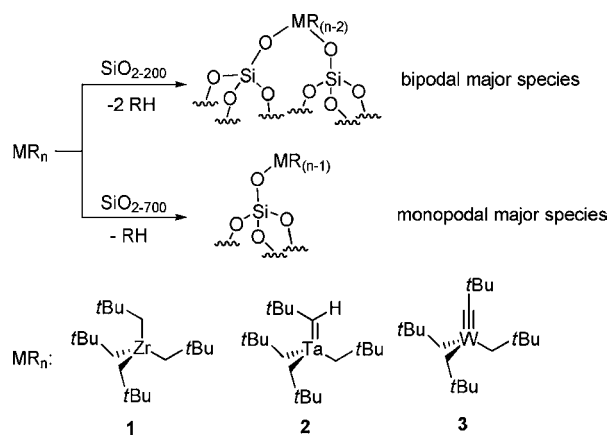
The MQ MAS spectrum of SiO₂*₋₂₀₀ allows the separation of Si–O–Si and SiOH signals (Figure 2c). The silanol region features a signal with a major symmetrical component (–5 ppm) along with a broader signal spanning toward higher chemical shifts. This parallels the observations made on the J-HMQC spectrum, namely a combination of “isolated” and vicinal silanols signals. Regarding the siloxanes, the MQ MAS experiment gives some insight on the composition of the monodimensional signal. A major contribution (spanning from

35 to 12 ppm) with large C_Q (*vide infra*) is present, most probably originating from several ^{17}O environments (differing in their local structure). The range of C_Q values for the main Si–O–Si contribution is evaluated at an upper value of 5 MHz, as deduced from extracted rows, which is in line with the data reported in the literature.^{15,17} The Si–O–Si pattern indicates occurrence of several structural types, which give rise to signals that cannot be spectroscopically separated, despite the high field (18.8 T). This illustrates both the complexity related to the use of an amorphous system and the high sensitivity of the ^{17}O nucleus to the local parameters (despite similar composition, siloxane signals are affected by subtle variations in bond lengths and angles, as well as by neighbor configurations). As was observed by Clark et al., the quadrupolar coupling constant seems to slightly decrease with increasing ^{17}O chemical shift.¹⁸ A minor component (about 10% of the siloxane signal) is observed as a chemical shift distributed signal from 40 to 30 ppm. In this case, the ^{17}O nuclei do not give rise to quadrupolar line shape. As so far in the literature bridging oxygens in silica-related materials feature C_Q close to 5 MHz, the nature of the present signal remains to be determined.

2. ^{17}O NMR Studies on Organometallic Species Grafted on $\text{SiO}_2^{*,-700}$. The use of ^{17}O MAS NMR for characterization of energy related and catalytic materials has mainly focused on crystalline and semicrystalline systems.⁷ However, studies on disordered materials are much more challenging, as demonstrated in the case of glassy materials.⁶ As the vast majority of heterogeneous catalysts involve non-structured materials, this confers an additional challenge to their study through a ^{17}O NMR approach. To increase our chances to collect significant data, we chose to focus on a class of catalysts of well-understood structure obtained from rationalized procedures. In this context, surface organometallic chemistry (SOMC) of hydrocarbyl transition metal derivatives is an approach that allows formation of well-defined surface species depending on the state of the silica surface.¹⁹ On a mildly dehydroxylated support such as SiO_2^{200} , mostly bipodal species (i.e., featuring two $\equiv\text{Si}-\text{O}-\text{M}$ bonds) are formed, while highly dehydroxylated silica such as SiO_2^{700} affords monopodal species (with a single siloxide $\equiv\text{Si}-\text{O}-\text{M}$ bond) (Scheme 2).

Grafting on silica dehydroxylated at 700 °C has been reported to provide high selectivity, affording well-defined

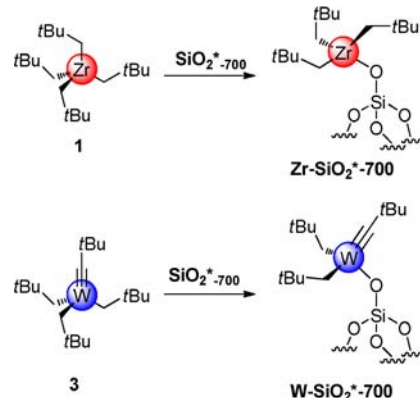
Scheme 2. Overall Reactivity of Silica toward Organometallic Complexes and Selected Examples



monopodal species thanks to the sole presence of isolated silanol groups on the surface. Indeed, grafting of zirconium tetraalkyl ([ZrNp₄], **1**, Np = CH₂tBu), tantalum trisalkyl-alkylidene ([Ta(=CHtBu)Np₃], **2**) and tungsten trisalkyl-alkylidene ([W(=CtBu)Np₃], **3**) proceeds to the formation of singly bound species [(≡SiO)ZrNp₃], [(≡SiO)Ta(=CHtBu)Np₂] and [(≡SiO)W(=CtBu)Np₂], as shown by combination of elemental and mass balance analyses, solid-state ^1H and ^{13}C MAS NMR, and EXAFS studies.²⁰ These have been designated as well-defined species, on the basis of these cumulated evidence. However, very little information can be extracted from these techniques, regarding the degree of interaction between the support and the grafted fragment: the average number of Si–O–M bonds can be extracted from elemental and mass balance analyses, and the presence of closer siloxane (estimates of quantification and distance) can be proposed from EXAFS, for instance. As amorphous silica presents a wide range of silanol local environments beyond the first approximation as vicinal or “isolated”, it is expected that different surface species of similar stoichiometry but different second coordination sphere are present, with non-negligible impact on catalytic performances.

We thus proceeded to the grafting of **1** and **3** on $\text{SiO}_2^{*,-700}$. This afforded Zr– $\text{SiO}_2^{*,-700}$ and W– $\text{SiO}_2^{*,-700}$, respectively (Scheme 3). In the ^{17}O NMR spectrum of zirconium-based

Scheme 3. Grafting of **1 and **3** on $\text{SiO}_2^{*,-700}$**



Zr– $\text{SiO}_2^{*,-700}$, the Si–O–Zr signal appears at about 212 ppm, and the siloxanes resonate at 60–10 ppm (Figure 4a).²¹ According to the information from infrared spectroscopy, no signals of silanol are observed, in line with a full consumption. Similarly, the W– $\text{SiO}_2^{*,-700}$ spectrum that comprises supported W species features a Si–O–W signal as a weak peak centered at 149 ppm and a Si–O–Si peak similar to that seen for Zr– $\text{SiO}_2^{*,-700}$ (Figure 4b). Furthermore, no SiOH signals are observed in either case, as confirmed with infrared data showing complete silanol consumption.

The ^{17}O MAS NMR spectrum (Figure 4c) recorded at lower magnetic field ($B_0 = 9.4$ T) on W– $\text{SiO}_2^{*,-700}$ allows assessment of the origin of the apparent symmetry of the siloxane signal and obtainment of some information on the origin of the width of the Si–O–M peak (M = W, Zr). As the second-order quadrupolar broadening (in ppm) is inversely proportional to the square of the B_0 field, recording at lower field exacerbates quadrupolar coupling effects. The significant broadening of the siloxane signals most probably resulting from overlapping of several oxygen sites thus accounts for the high quadrupolar

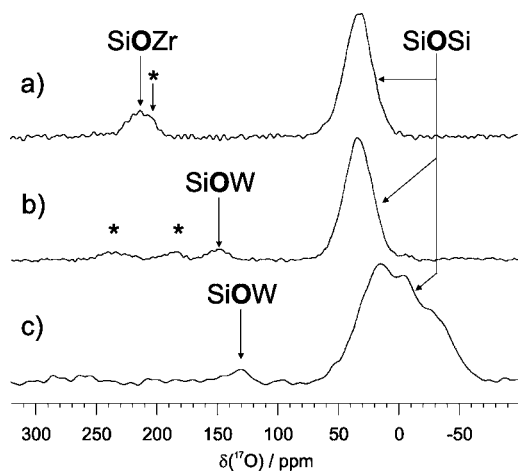


Figure 4. ^{17}O MAS NMR spectra of (a) $\text{Zr-SiO}_2^{*-.700}$ (18.8 T, $n_s = 44592$), (b) $\text{W-SiO}_2^{*-.700}$ (18.8 T, $n_s = 16384$), and (c) $\text{W-SiO}_2^{*-.700}$ (9.4 T, $n_s = 40960$). Conditions: $rd = 2$ s, MAS rate = 19 kHz (a) or 21 kHz (b and c). Asterisks indicate positions of spinning side bands.

coupling associated with these oxygen environments. The upfield line broadening allows for the evaluation of the quadrupolar coupling constant at an upper estimate of about 5 MHz. The slight upfield displacement of the Si–O–M signal (130 ppm at 9.4 T compared to 149 ppm at 18.8 T) is representative of a non-negligible quadrupolar coupling constant, even though it is smaller than that observed for siloxanes.

3. ^{17}O NMR Studies on Organometallic Species Grafted on $\text{SiO}_2^{*-.200}$. Surface organometallic chemistry on $\text{SiO}_2^{*-.200}$ is less straightforward than that conducted on $\text{SiO}_2^{*-.700}$, as expected from the several types of silanol groups (in terms of local structure) present on its surface, which may lead to the formation of mixtures of species.²² The high density of silanol induces a strong tendency to form bipodal species.²³ Several hybrid materials were prepared and characterized, by grafting **1**, **2**, and **3** (among others) on $\text{SiO}_2^{*-.200}$, and the distribution of surface species was studied, by means of elemental analysis, grafting reaction stoichiometry assessment, and EXAFS (Scheme 4). In these cases, the distribution of the SiO–M–OSi angles is expected to be significant, due to the intrinsic heterogeneity of the amorphous support. Therefore, the deep characterization of these materials is still an open, challenging task.

To probe these matters, the grafting of **1**, **2**, and **3** was carried out on $\text{SiO}_2^{*-.200}$. The nonlabeled analogous materials have already been studied through several spectroscopic techniques.^{20a,b,24} Significant differences in their reactivity toward silica are known, for instance, between the more oxophilic Zr and Ta derivatives on one hand and their W analogue on the other hand, which is less oxophilic and less reactive toward silanols. This translates into uncomplete silanol consumption in the case of **3** (and of **2**, to a lesser extent), as exemplified by IR spectroscopy, as well as in the lesser thermal stability of the SiO–W bond upon thermal treatment.

For $\text{Zr-SiO}_2^{*-.200}$, $\text{Ta-SiO}_2^{*-.200}$, and $\text{W-SiO}_2^{*-.200}$, ^{17}O MAS NMR spectra display signals accounting for Si–O–M, Si–O–Si, and SiOH, the latter in various proportions (Figure 5). The Si–O–M groups give rise to broad, featureless peaks centered around 225, 217, and 160 ppm for the Zr, Ta, and W systems, respectively.²¹ The Si–O–Si region is unchanged compared to $\text{SiO}_2^{*-.200}$ at first sight (*vide infra*).

Scheme 4. Grafting of **1**, **2**, and **3** on $\text{SiO}_2^{*-.200}$ and the Postulated Major Surface Species

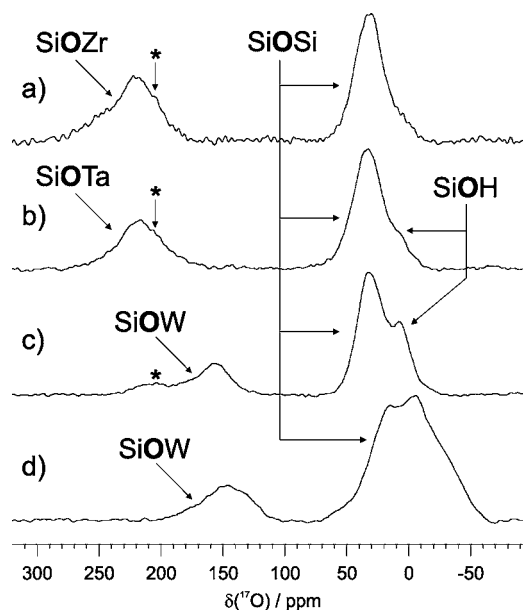
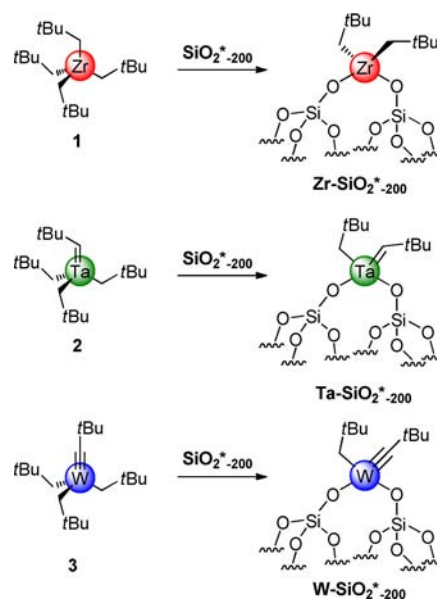


Figure 5. ^{17}O MAS NMR spectra of (a) $\text{Zr-SiO}_2^{*-.200}$ (18.8 T, $n_s = 20480$), (b) $\text{Ta-SiO}_2^{*-.200}$ (18.8 T, $n_s = 16384$), (c) $\text{W-SiO}_2^{*-.200}$ (18.8 T, $n_s = 17156$), and (d) $\text{W-SiO}_2^{*-.200}$ (9.4 T, $n_s = 115664$). Conditions: $rd = 3$ s and MAS rate = 19 kHz, except for part d, for which $rd = 2$ s and MAS rate = 21 kHz. Asterisks indicate positions of spinning side bands.

The MQ MAS spectra of $\text{Ta-SiO}_2^{*-.200}$ and $\text{W-SiO}_2^{*-.200}$ provide finer description for each of the regions of the ^{17}O environments (Figure 6). The silanol and siloxane regions are very similar for both materials. In the case of the SiOH, the spectrum of the tungsten derivative is more informative, as higher silanol content is present in the sample. In this case, the signal is dominated by a chemical shift distribution from -6 (free silanols) to 15 ppm, and it can be divided into two groups centered on about 3 and 9 ppm (respectively **SiOH-1** and **SiOH-2**). In the case of the tantalum-derived material, MQ MAS allows for observation of the weak (MAS) signal of the

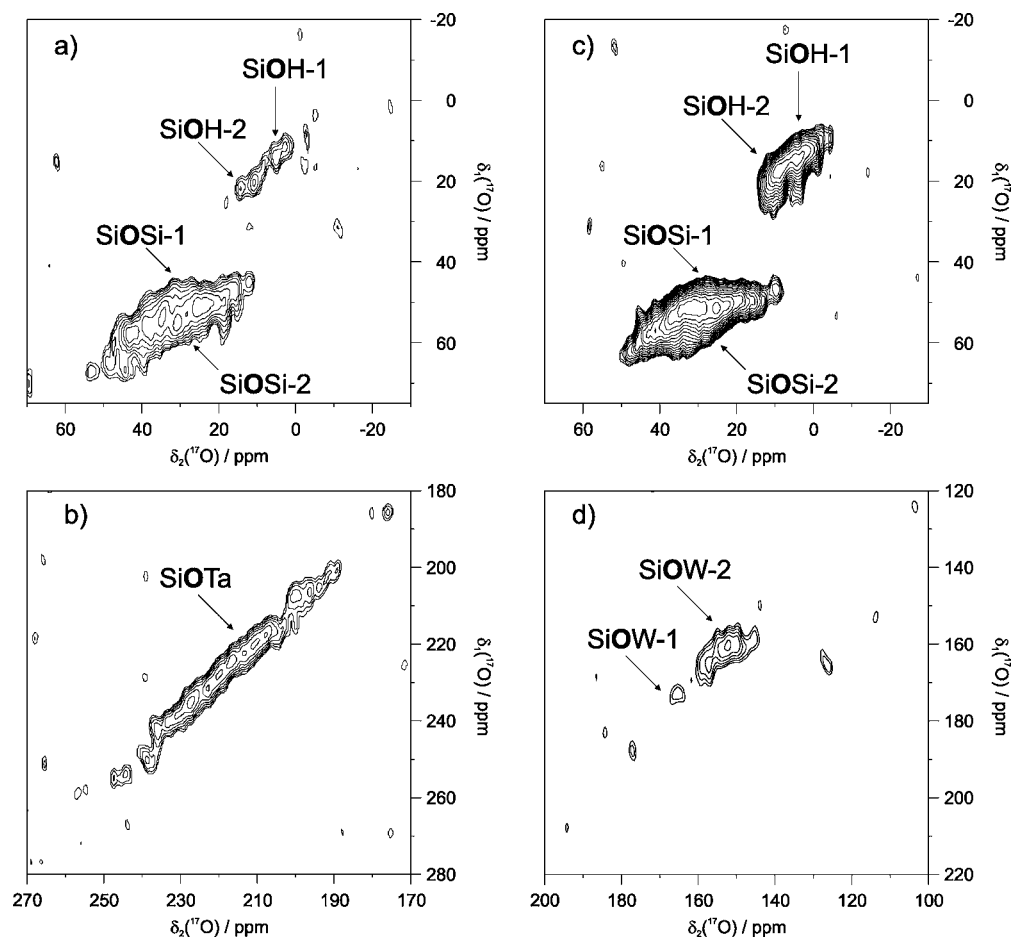


Figure 6. ^{17}O MQ-MAS NMR spectra at 18.8 T of (a and b) $\text{Ta-SiO}_2^{*_{-200}}$ and (c and d) $\text{W-SiO}_2^{*_{-200}}$. Conditions: ($\text{Ta-SiO}_2^{*_{-200}}$) $n_s = 6400$, $rd = 1$ s, $t_1 = 36$, acquisition time = 64 h, MAS rate = 20 kHz. ($\text{W-SiO}_2^{*_{-200}}$) $n_s = 7200$, $rd = 1$ s, $t_1 = 42$, acquisition time = 84 h, MAS rate = 20 kHz.

silanols, and despite small signal sensitivity, the same configuration as in $\text{W-SiO}_2^{*_{-200}}$ is also found (i.e. the two massifs at 3 and 9 ppm for SiOH-1 and SiOH-2 , respectively). The siloxane signal is similar for both samples. It is more complex than the SiOH one, as expected from the comparison of the 18.8 and 9.4 T monodimensional spectra of the tungsten derivative (Figure 5c,d). The major signal (SiOSi-1) is dominated by second-order quadrupolar broadening, with a chemical shift corrected from the second-order contribution of about 35 ppm. This is very similar to that observed for pristine $\text{SiO}_2^{*_{-200}}$. Another contribution (SiOSi-2), distributed along the diagonal, with an averaged chemical shift value of 40 ppm, originates from chemical shift-distributed siloxane signals.

One of the most striking differences when comparing the spectra of $\text{W-SiO}_2^{*_{-200}}$ and $\text{Ta-SiO}_2^{*_{-200}}$ to that of $\text{SiO}_2^{*_{-200}}$ is the modification of the siloxane massif. Indeed, the highly quadrupolar SiOSi-1 component is still present but is now the minor component, as it is observed together with the large distributed SiOSi-2 ensemble pointing toward high ^{17}O chemical shift with concomitant slight signal narrowing. This must derive from the perturbation induced by the organo-metallic fragment.

Regarding the Si–O–M region, the tantalum- and tungsten-based materials give rise to slightly different signals. For $\text{Ta-SiO}_2^{*_{-200}}$, the MAS spectrum can be interpreted as deriving from a single component (SiOTa , Figure 6b), centered at about 220 ppm and showing a large chemical shift distribution. On the other hand, for $\text{W-SiO}_2^{*_{-200}}$, the MAS spectrum (Figure

5d) shows the same high field displacement at 9.4 T compared to that for $\text{W-SiO}_2^{*_{-700}}$. The signal maximum shifts from 160 to 146 ppm, which is indicative of the presence of a quadrupolar effect in the signal (See Figure S4 in the Supporting Information). The broad MAS signal (Figure 5c) can be decomposed on the basis of MQ-MAS observations into two components: a site (SiOW-1) centered at 152 ppm dominated by a quadrupolar coupling effect and a second site (SiOW-2) dominated by a chemical shift distribution spanning from 200 to 120 ppm (Figure 6d; see the Discussion section).

To gain further information on the spatial configuration on the surface species of $\text{W-SiO}_2^{*_{-200}}$, we resorted to the D-HMQC experiment that relies on heteronuclear dipolar interactions to probe the proximity between ^{17}O and ^1H sites (Figure 7).²⁵ Correlation signals appear for only Si–OH and Si–O–Si environments. The chemical shift distribution of the main Si–O–W signal may prevent efficient echo manipulation and therefore prevent the corresponding HMQC signal to be detected. The silanol ^{17}O nuclei mainly correlate with protons located in the 1.7–2.7 ppm range as a nonsymmetrical pattern. The Si–O–Si ^{17}O signals are correlated to protons of the alkyl groups. No significant correlation spots are observed between siloxanes and silanols.

DISCUSSION

Following the data presented in the Results section, each of the oxygen environments, namely silanols, siloxanes, and metal

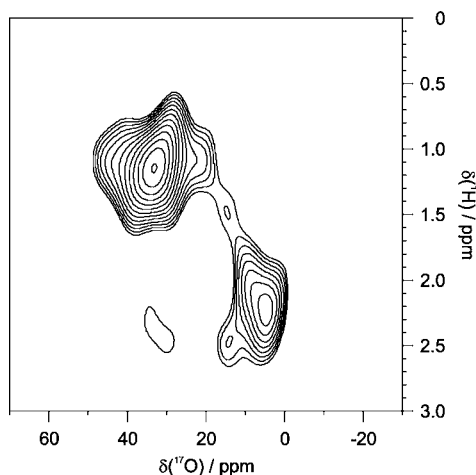


Figure 7. ^{17}O HMQC MAS NMR spectrum at 18.8 T of W-SiO_2^{*-200} ($n_s = 12800$, $rd = 1.5$ s, $t_1 = 16$, MAS rate = 21 kHz, acquisition time = 85 h).

siloxides, gives rise to diagnostic ^{17}O NMR spectroscopic features that provide the most valuable structural information on the topology of the heterogeneous catalyst surface.

1. Silanol Region. On the materials derived from grafting the selected organometallic precursors **1**, **2**, and **3**, only those grafted on SiO_2^{*-200} feature residual silanols. The trends observed by infrared spectroscopy are similar to those presently observed through ^{17}O NMR: while only small quantities of Si–O–H are left in the Zr and Ta cases, a significant proportion appears on the W-SiO_2^{*-200} material. Interestingly, in this case, the MAS signal is shifted toward higher chemical shifts ($\Delta\delta$ of about 12.5 ppm). More detailed information can be obtained by careful analysis of the MQ MAS and HMQC spectra. In the MQ MAS spectra of W-SiO_2^{*-200} and Ta-SiO_2^{*-200} (Figure 6), two main types of residual silanols, SiOH-1 and SiOH-2, can be distinguished, differing in their chemical shifts (respectively 3 and 9 ppm). Interestingly, by comparing the silanol region in the MQ MAS and in the D-HMQC spectra of W-SiO_2^{*-200} , it appears that the two sites correspond to different SiOH groups that could not be distinguished in the ^1H and ^{17}O MAS NMR spectra (Figure 8). In the D-HMQC spectrum, the SiOH-1 ^{17}O signal (centered at about 5 ppm) correlates with protons spanning from 2.6 to 1.8 ppm. The SiOH-2 distribution (14 to 6 ppm in ^{17}O dimension, 2.2 to 1.5 ppm in ^1H dimension) is such that the ^1H and ^{17}O chemical shifts are inversely related: the ^{17}O deshielding is associated with ^1H shielding. Furthermore, within this pattern, the ^1H and ^{17}O chemical shift trend differs from the observations made in the SiO_2^{*-200} J-HMQC spectrum, in which interacting (H-bonded) silanols tend to have downfield shifted ^1H and ^{17}O NMR signals. The chemical shift of the ^{17}O nucleus is highly sensitive to medium- to long-range effects, whereas protons are much less affected by screening effects. This means that the considered protons (related to SiOH-2 sites) are not involved in H-type bonding but are rather to be considered as being in interaction with alkyl fragments, as already observed in the case of grafted ($\equiv\text{SiO}$)Ta(Cp*)Me₃ fragments ($\delta = 0.6$ ppm for residual interacting silanols).²⁶ When compared to the corresponding MQ MAS pattern, the more perturbed SiOH-2 ^{17}O nuclei (compared to free silanols at -6 ppm) correlate to the more highfield shifted protons and, therefore, to shorter distances to organometallic fragments. Remarkably, such information could

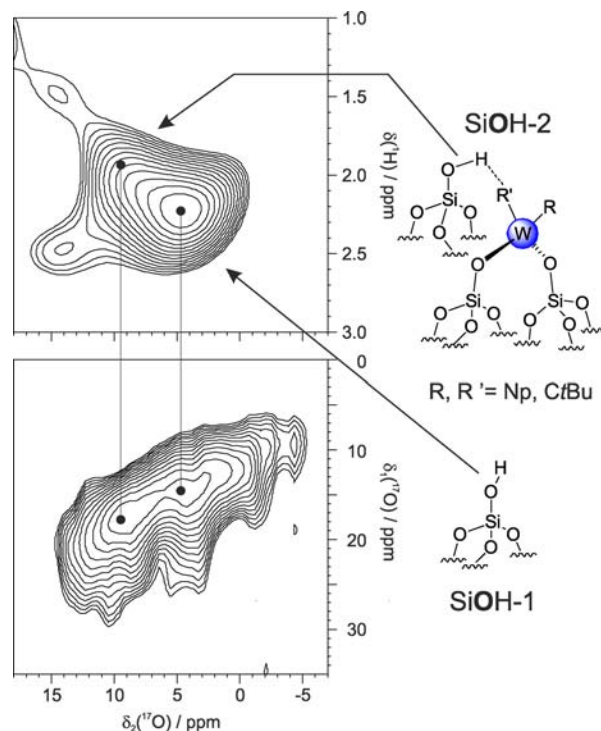


Figure 8. Comparison of the silanol region of the HMQC (top left) and MQ MAS (bottom left) of W-SiO_2^{*-200} and proposed assignments.

not be extracted from ^1H – ^1H correlation methods, as the silanol ^1H signal is too broad: by benefiting from ^{17}O resolution and large chemical shift dependence (the silanol signals span over 20 ppm), we are thus able to extract information on the SiOH's neighbors.

We propose that the first pattern (SiOH-1, centered at about 5 ppm/2.3 ppm in respective $^{17}\text{O}/^1\text{H}$ dimensions) originates from silanol groups without interaction with organometallic fragments and that the second distribution (SiOH-2, centered at 9 ppm/1.9 ppm in respective $^{17}\text{O}/^1\text{H}$ dimensions) is due to the silanols located in the second coordination sphere of the metal, featuring weak interactions between protons of the silanols and the tungsten alkyl fragments (Figure 8). The observed ^1H shielding, as opposed to the deshielding effect for the H-bonded silanols in SiO_2^{*-200} , pleads for the involvement of van der Waals interactions. We also exclude from the low ^{17}O CS difference, the formation of SiOH–tungsten adducts, where the oxygen center would bind the metal, as already proposed.²⁷ The fact that no correlations are observed between the silanol oxygens and the alkyl fragments in the HMQC spectrum may also mean that they are not within correlating distance and, therefore, that the oxygens nuclei are not directly involved in the above-mentioned silanol–alkyl interaction. In a related example, namely **3** grafted on $\gamma\text{-Al}_2\text{O}_3$, both the IR detected shift in $\nu(\text{OH})$ and ^{13}C deshielding have been assigned to interactions between [Al]–O–H and alkyl groups of the organometallic surface fragments, thanks to supportive theoretical DFT studies.²⁸ In our example, structural information directly related to the involved surface hydroxyls was extracted from combined 2D spectrum data.

2. Siloxane Region. When considering the 9.4 T ^{17}O MAS spectra of W-SiO_2^{*-200} (Figure 5d) and W-SiO_2^{*-700} (Figure 4c), one can first note that the spectral line width of the Si–O–

Si signals is dominated by the large quadrupolar coupling associated with the surface siloxane oxygens. Both materials feature similar full width at half-maximum, and differ in that the $W-SiO_2^{*-.200}$ spectrum comprises a silanol signal at -5 ppm. A better resolution is provided by MQ MAS at 18.8 T, recorded for $W-SiO_2^{*-.200}$ and its tantalum counterpart, $Ta-SiO_2^{*-.200}$. As previously mentioned, both materials feature similar 2D patterns in the siloxane region, with significant changes from pristine $SiO_2^{*-.200}$ silica. Introduction of the organometallic center significantly affects a large share of the siloxanes. As appears in Figure 9, the main SiOSi component (SiOSi-1) is

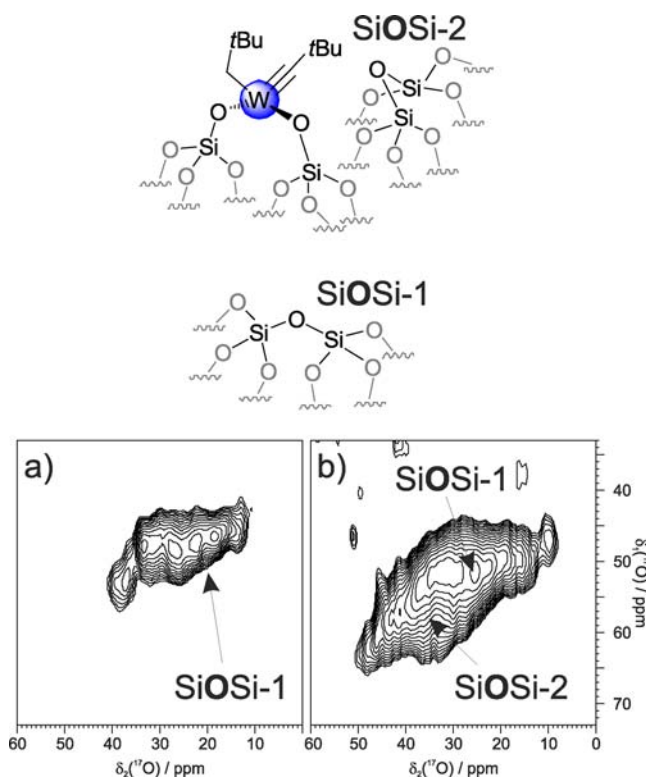


Figure 9. Siloxane region of the MQ MAS spectra of (a) $SiO_2^{*-.200}$ and (b) $W-SiO_2^{*-.200}$, and proposed assignments.

dramatically affected by the tungsten complex grafting. Indeed, a dominant component (SiOSi-2) appears in the MQ MAS spectra of $W-SiO_2^{*-.200}$ and $Ta-SiO_2^{*-.200}$, as chemical shift distributed, that retains high C_Q though lower than that of SiOSi-1. Extracted MQ MAS slices clearly illustrate this (Supporting Information Figure S8). The nature of the SiOSi-2 siloxanes contribution can be discussed on these bases: their chemical shift is strongly affected, from 40 ppm in SiOSi-1 to 50 ppm (higher value of the distributed signal). Remarkably, along this chemical shift distribution, the quadrupolar coupling constant remains quasi-unchanged, reflecting with high degree of precision that the covalent bridging nature of the siloxane is retained (very small variations in distance and bond angle; see the work of Clark et al.¹⁸). The C_Q upper estimate only slightly decreases from about 5.3 MHz in SiOSi-1 to 5.1 MHz in SiOSi-2 (see Supporting Information Table S1). This is a strong indication that the considered oxygens are not directly bound to the metal center, namely, that siloxanes are not coordinated to the metal center, as this would dramatically affect both chemical shift and quadrupolar coupling constants. The observed effects on CS are thus

electrostatic in origin and are most probably due to long- to medium-range perturbations originating from the grafting of the organometallic center, reflecting the metal–oxygen distance within the second coordination sphere. Furthermore, DFT calculations indicate that siloxane binding on the metal is not effective: W(VI) do not bear suitable accessible orbitals, contrarily to what is observed in lanthanide surface chemistry.²⁹

In the $^1H-^{17}O$ HMQC spectrum, the Si–O–Si ^{17}O only correlate with the alkyl fragments' protons. By comparing the MQ and HMQC MAS spectra, it appears that all Si–O–Si types show dipolar coupling with alkyl protons. However, the HMQC experiment is not selective enough to differentiate between the different (SiOSi-1 and SiOSi-2) Si–O–Si types regarding their interaction with alkyl groups, whether CH_2 or CH_3 .

3. Metal–Siloxide Region. Insight into the nature of the metal-to-support bond itself is of prime importance, as it is the main point of interaction between the anchored catalytic site and the host material. Regarding this, our specific labeling of silanols offers a unique chance to reach such type of information, with a degree of confidence and precision that is not readily available through other spectroscopic methods.

In the $W-SiO_2^{*-.700}$ and $Zr-SiO_2^{*-.700}$ MAS spectra (Figure 4), the metal–siloxide oxygens give rise to peaks at characteristic chemical shifts (149 and 212 ppm, respectively).²¹ The chemical shifts are apparently moderately distributed (165–125 ppm for $W-SiO_2^{*-.700}$ and 230–190 ppm for $Zr-SiO_2^{*-.700}$). Though no quadrupolar line shapes are observed, recording of the spectrum of $W-SiO_2^{*-.700}$ at 9.4 T (Figure 4b and c) indicates that these ^{17}O environments present quadrupolar character (see DFT calculations below). From the postulated structure, namely an organometallic species with a single metal–support bond, it is expected that although significant mobility around the Si–O–M fragment will occur, the main structure remains unchanged: the Si–O–M angle and corresponding distances should be restricted to a narrow range, leading to a dominant contribution from the quadrupolar interaction. Indeed, DFT calculations on a monosiloxide model species of $[(\equiv SiO)W(\equiv CtBu)Np_2]$ (Figure 10) give as a result CS, C_Q and η_Q values of 143 ppm, 4.08 MHz, and 0.22, respectively. Input of the C_Q and η_Q values with a chemical shift

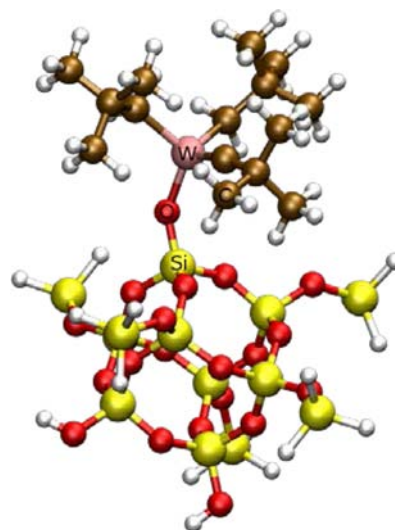


Figure 10. DFT calculated model of monografted species.

adjusted to the experimental value results in the calculated spectrum presented in Figure 11d. Obviously, further

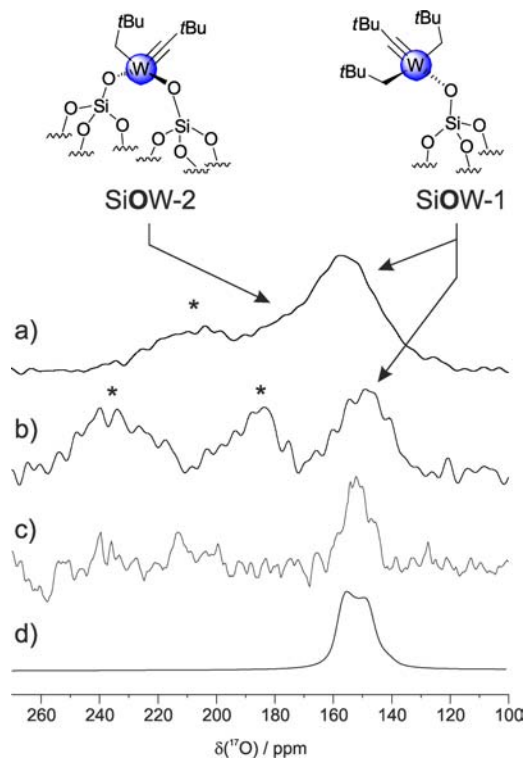


Figure 11. (a) MAS spectrum of $W\text{-SiO}_2^{*-.200}$; (b) MAS spectrum of $W\text{-SiO}_2^{*-.700}$; (c) Extracted row ($\delta 1 = 160$ ppm) from the MQ MAS spectrum of $W\text{-SiO}_2^{*-.200}$; and (d) DFT calculated spectrum of the $[(\equiv\text{SiO})\text{W}(\equiv\text{CtBu})\text{Np}_2]$ model. Asterisks indicate positions of spinning side bands.

distribution is at hand, which is not taken into account in the calculated spectrum, as will be discussed later with MQ MAS. Overestimation of CS by DFT calculation is often observed and would require calibration with an internal reference, as ^{17}O CS of silanol groups without interaction with organometallic fragments.

Regarding materials prepared from $\text{SiO}_2^{*-.200}$, the MAS spectra of Zr-, Ta-, and W-modified materials are markedly different compared to those recorded on $\text{SiO}_2^{*-.700}$: the Si–O–M signals appear as featureless resonances again centered at chemical shifts characteristic of those found in the literature (225, 217, and 160 ppm, respectively).²¹ Interestingly, the deshielding is associated with the electrophilic character of the metal. The nonsymmetrical line shape of the Si–O–M signal of the Zr- and W-derived materials motivated further investigation. First of all, recording the MAS spectrum of $W\text{-SiO}_2^{*-.200}$ at 9.4 T reveals that the Si–O–W signal is less affected than that of the siloxane, as the signal is only shifted from 160 to 146 ppm. This is due to a dominant distribution of chemical shift. Only the right part of the signal shows line shape modification at lower magnetic field. This is an evidence of involvement of an additional component that features a stronger quadrupolar character.

The MQ-MAS spectra (Figure 6) were recorded for the two extreme cases of Si–O–M signals ($\text{Ta-SiO}_2^{*-.200}$ as purely CS-distributed and $W\text{-SiO}_2^{*-.200}$ as mixture of CS-distributed and quadrupolar components). Striking differences confirm the MAS-derived conclusions: whereas $\text{Ta-SiO}_2^{*-.200}$ gives rise to a

purely distributed signal along an axis of slope 1, $W\text{-SiO}_2^{*-.200}$ features a weak distributed component (SiOW-2) together with a more intense (as more responsive to MQ MAS) quadrupolar component, SiOW-1. The major component SiOW-2 is purely dominated by a chemical shift distribution (from 200 to 120 ppm). The more strongly quadrupolar-coupled site SiOW-1 centered at 152 ppm features a C_Q value of 3.3 MHz from the best fit simulation of a MQ MAS extracted row, and is slightly CS distributed (Figure 11c). A direct assignment for this signal can be proposed as the monosiloxide species $[(\equiv\text{Si}-\text{O})\text{W}(\equiv\text{CtBu})(\text{Np})_2]$, observed in $W\text{-SiO}_2^{*-.700}$. Indeed, the MQ MAS extracted row NMR features closely match the theoretical values for this species. A slight chemical shift difference between the $W\text{-SiO}_2^{*-.200}$ and $W\text{-SiO}_2^{*-.700}$ SiOW-1 (monopodal) sites (centered at 152 and 149 ppm, respectively) may result from long distance interactions, as the surface grafting density is higher on $\text{SiO}_2^{*-.200}$ than on $\text{SiO}_2^{*-.700}$. On the other hand, the broad, major SiOW-2 signal is assigned to bipodal species $[(\equiv\text{Si}-\text{O})_2\text{W}(\equiv\text{CtBu})(\text{Np})]$. In the MQ MAS spectrum of $W\text{-SiO}_2^{*-.200}$, this resonance does not give rise to a significant signal. Indeed, the large chemical shift range for SiOW-2 accounts for a statistical distribution of geometrical (structural) parameters. In these environments, the quadrupolar effect is most probably quenched by the use of high field and blurred by this distribution.

DFT calculations on a bipodal model species of $[(\equiv\text{Si}-\text{O})_2\text{W}(\equiv\text{CtBu})(\text{CH}_2\text{tBu})]$ give as a result CS, C_Q , and η_Q values of 165 and 175 ppm, 4.14 and 4.27 MHz, and 0.70 and 0.60, respectively for O_a and O_b , when the grafting reaction takes place on two unconnected vicinal silanol groups (Figure 12b). However, the grafting reaction can also take place on two

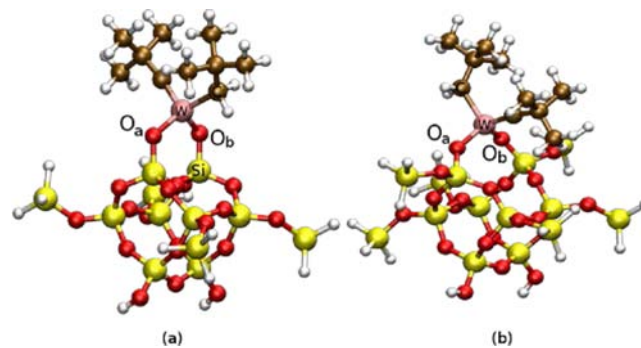


Figure 12. DFT calculated models of bigrafted species. (a) Vicinal silanol groups connected by a siloxane bridge. (b) Unconnected vicinal silanols.

vicinal silanol groups connected by a siloxane bridge (Figure 12a), which give as a result CS, C_Q and η_Q values of 202 and 191 ppm, 4.35 and 4.43 MHz, and 0.69 and 0.63, respectively, for O_a and O_b . Taking into account these structures enlarges the distribution of ^{17}O NMR data, in agreement with the experimental $W\text{-SiO}_2^{*-.200}$ observation.

These spectroscopic elements are directly connected to the structural features of the two types of grafted species. The monografted species is present on the surface as entities that have very similar local structures: the Si–O and O–W distances and Si–O–W bond angles are expected to vary in a narrow range, and the main changes will result from outer coordination sphere effects. This leads to the low broadening of the Si–O–W signal in $W\text{-SiO}_2^{*-.700}$ and the presence of a slightly CS-distributed quadrupolar site in the MQ MAS spectrum of $W\text{-SiO}_2^{*-.200}$.

SiO_2^{*200} (both accounting for SiOW-1 sites). On the other hand, the bipodal $[(\equiv\text{Si}-\text{O})_2\text{W}(\equiv\text{CtBu})(\text{CH}_2\text{tBu})]$ surface species is expected to feature a wide variety of geometries due to the support's intrinsic heterogeneity. This results in variation of the surface bisiloxide chelate, which features wide ranges of O–W–O and Si–O–W angles and Si–O and O–W distances. This correlation is also found theoretically. For instance, the two calculated models of bigrafted species display an important variation of the ^{17}O NMR data (0.29 MHz on C_Q and 40 ppm on CS) as well as a large variation of the O–W–O (from 121° to 140°) and Si–O–W angles (from 111° to 115°) according to the bipodal coordination of the tungsten complex on a rigid structure (Figure 12a) or on a most flexible structure (Figure 12b), respectively. This structural diversity induces a wide distribution of chemical shifts. In this case, the high magnetic field quenches the quadrupolar distribution and exacerbates the chemical shift distribution, resulting in a Gaussian line shape in a large proportion for the SiOW-2 signal.

In a further step, after qualitative assessment of the metal siloxide signal, we also carried out its quantitative analysis to extract surface (mono- vs bipodal) species proportions. This was done from the ^{17}O MAS spectrum on the following bases: the bipodal species signal (SiOW-2) is fitted as a Gaussian line at 163 ppm, with a full width at half-maximum of 37 ppm. DFT calculated values for the monopodal site (SiOW-1) were used to provide best estimates using an exponentially broadened quadrupolar line shape. From these elements, the molar ratio for the bipodal and monopodal species amounts to about 75–25, respectively. Previous studies on W-SiO₂₋₂₀₀ prepared with nonprecalcined Aerosil SiO₂₋₂₀₀ demonstrated that the bipodal species is the major species, with only a small amount of monopodal analogue.^{20c} However, it is known that rehydroxylation of a calcined silica material is a process that does not fully regenerate the same type of silanols population.³⁰ The herein described labeling procedure for the ^{17}O -tagged silica support goes through a 1000 °C annealing step followed by rehydration. It is thus to be expected that the resulting surface chemistry may subtly differ from what was described with noncalcined supports. Nevertheless, as shown in this case study, ^{17}O NMR is a reliable technique to directly assess the proportion between structurally close species. ^1H and ^{13}C NMR have been used in rare instances to this purpose;³¹ however, they cannot unambiguously distinguish between such closely structurally related species as mono- and bigrafted perhydrocarbyl fragments. Furthermore, Scott and co-workers have shown that unexpected bonding situations may well be expected from such a seemingly simple system as dehydroxylated silica:³² its surface chemistry can still provide surprises, and a sensitive technique such as ^{17}O NMR can definitively contribute to its better understanding.

4. Compared Input of ^{17}O NMR as a Novel Tool for Grafted Catalysts Studies. In summary, we have introduced a new approach to the study of heterogeneous catalysts, by use of ^{17}O nucleus as a NMR probe to investigate the very interface between an inorganic carrier and immobilized organometallic centers. Within this study, we gathered elements not only on the structure of the supported species but also on the nature of the metal-to-support interactions. As mentioned in the Introduction, the main classical techniques provide key elements to some of the surface species, whether or not organometallics (Table 1). More specifically, for the grafted organometallic catalysts considered here, while their output is considerable, their drawbacks can be summarized as follows:

Table 1. Compared Scopes of Surface Group Spectroscopic Studies

	IR	Raman	EXAFS ^a	^1H – ^{13}C NMR	^{17}O NMR
SiOH	X	X		X	X
SiOSi		X ^b	X		X
SiOM		X	X		X
MR _n	X	X	X	X	X ^c

^aRestricted to heavy elements. ^bInformation significantly blurred by bulk signal. ^cFrom heteronuclear correlations.

vibrational spectroscopies are mostly qualitative, EXAFS is strongly model-dependent, and ^1H and ^{13}C NMR are mainly restricted to grafted moieties. While these techniques are highly complementary, they do not provide precise and localized information on the structure of the interface between the host material and the organometallic fragments, namely the very surface of the catalytic material.

Our main findings are the following:

(1) It is possible to perform a selective ^{17}O surface labeling for such a widely used inorganic carrier as silica. We have shown that this host material (partially dehydroxylated at 200 and 700 °C) is amenable to ^{17}O (mono- and bidimensional) MAS NMR investigations, giving a detailed picture of the surface oxygen environments, thanks to the high sensitivity of ^{17}O NMR parameters to subtle structural changes.

(2) This was extended to the study of catalytically relevant hybrid materials prepared by grafting of organometallic complexes. The wealth of information that can be extracted by ^{17}O MAS NMR combined with DFT calculations is clearly exemplified in Table 2, which gathers extracted NMR data for all types of oxygen environments (silanols, siloxanes, and siloxides) found on the surface of both types of studied silica (SiO_2^{*200} and SiO_2^{*700}) and their corresponding tungsten-derived materials.

Thus, in this context, our specific ^{17}O surface labeling of silica associated with ^{17}O NMR proved to be very efficient. First degree of information can be drawn from chemical shift analysis, as silanols, siloxanes and metal siloxides are characterized by clearly distinct ranges ([15–20] ppm, [50–10] ppm and [270–130] ppm depending on the metal, respectively). Thus, in a single 1D ^{17}O MAS NMR spectrum, full picture of bonding situations and quantitative information can be efficiently obtained. Furthermore, more subtle effects modify NMR parameters, such as (distribution of) chemical shift and/or quadrupolar coupling constant, enabling to monitor structural variations at the molecular level. A higher degree of refinement can be achieved by resorting to high resolution (MQ MAS) and heteronuclear (HMQC) correlation techniques, combined with a theoretical chemistry approach that clearly enhances the confidence level of the conclusions.

On these grounds, information has been extracted using a combination of ^{17}O 1D and 2D NMR and DFT, which cannot be obtained by other established methods:

(1) Direct spectroscopic evidence for involvement of (structurally very similar) mono- and bis-grafted systems, instead of using an averaged value (from EXAFS or elemental analysis), with full support from DFT calculations. Direct speciation (quantification) is thus possible from a 1D spectrum.

(2) Proximity of various fragments as provided by the heteronuclear correlation method, such as the robust HMQC sequence (infrared shows, for instance, that silanol signals are

Table 2. Compared ^{17}O NMR Parameters for $\text{SiO}_2^{*-.200}$, $\text{SiO}_2^{*-.700}$ and the Corresponding Tungsten-Derived Materials

	SiOH	SiOSi	SiOM
$\text{SiO}_2^{*-.200}$	−5.8 ppm ^a (non- or weakly interacting) 10 to −20 ppm ^a (strongly interacting)	35 ppm, $C_Q > 5$ MHz ^b (SiOSi-1)	
$\text{SiO}_2^{*-.700}$	−7.4 ppm (noninteracting)	40–10 ppm ^c (SiOSi-1)	
W-SiO ₂ ^{*-.200}	3 ppm ^d (SiOH-1) 9 ppm ^d (SiOH-2)	35 ppm; C_Q , 5.3 MHz ^b (SiOSi-1)	163 ppm; C_Q , 4.1 MHz ^b (SiOW-1, monopodal species)
W-SiO ₂ ^{*-.700}		50–40 ppm; C_Q , 5.1 MHz ^b (SiOSi-2) about 50–10 ppm ^e (SiOSi-1 and SiOSi-2)	159 ppm ^e (SiOW-2, bipodal species) 157 ppm; C_Q , 4.1 MHz ^f (SiOW-1, monopodal species)

^aFrom J-HMQC spectrum. ^bParameters deduced from MQ MAS spectrum, chemical shift corrected from second order contribution. ^cChemical shift region deduced from MAS spectrum. ^dChemical shift deduced from D-HMQC and MQ MAS spectra. ^eAverage value from a 200–120 ppm distribution. ^fDeduced from combined DFT and experimental results.

shifted, but without giving any structural details, while ^{17}O – ^1H HMQC can provide such information).

(3) Existence or absence of metal-coordinated siloxane bridges and of residual silanols, for instance. No other technique can provide such information on the molecular level: the EXAFS technique gives averaged value, as mentioned above, and is silent toward light elements such as (silanols') hydrogen.

CONCLUSION

In conclusion, for the first time, we report the use of ^{17}O MAS NMR as a spectroscopic tool that allows probing the interaction of the silica surface with diamagnetic metal centers. This was achieved by combining an original, selective ^{17}O enrichment method with a well-controlled preparation of heterogeneous catalysts. ^{17}O MAS, MQ MAS, and D-HMQC NMR spectra were recorded with an exploitable signal-to-noise ratio thanks to the use of high magnetic field. Most importantly, experimental data were supported by DFT calculations, which helped to reach a higher level of understanding. Key information was extracted for each of the various oxygen environments: silanols, siloxanes, and metal-bound siloxides. This very promising approach can be applied to a wide range of silica-supported catalysts. Thus, ^{17}O NMR as a novel tool for the deep characterization of supported species will foster better understanding of metal–support interactions, a major issue in heterogeneous catalysts molecular structure understanding and key to access improved catalytic performances.

EXPERIMENTAL SECTION

Materials and Methods. All experiments were carried out by using standard Schlenk and glovebox techniques. Solvents were purified and dried according to standard procedures. Complexes **1**, **2**, and **3** and materials $\text{Zr-SiO}_2^{*-.200}$, $\text{Zr-SiO}_2^{*-.700}$, $\text{Ta-SiO}_2^{*-.200}$, $\text{W-SiO}_2^{*-.200}$, and $\text{W-SiO}_2^{*-.700}$ were prepared following literature methods.^{20,24} IR spectra were recorded on a Nicolet 6700 FT-IR spectrometer by using a DRIFT cell equipped with CaF_2 windows. The samples were prepared under Ar within a glovebox. Typically, 64 scans were accumulated for each spectrum (resolution 4 cm^{-1}).

Solid-state NMR spectra were acquired on a Bruker Avance III 800 spectrometer (^1H , 800.13 MHz; ^{17}O , 108.48 MHz) and on a Bruker Avance II 400 spectrometer (^1H , 400.13 MHz; ^{17}O , 54.24 MHz). For ^1H experiments, the spinning frequency was 20 kHz, the recycle delay was 5, and 16 scans were collected using a 90° pulse excitation of 2.25 μs . The ^{17}O MAS NMR spectra at 18.8 T were acquired at spinning frequencies ranging from 15 to 21 kHz (3.2 mm rotor diameter) to avoid overlapping of spinning sidebands with CS resonances. The ^{17}O MQMAS spectra³³ were collected using the Z-filter sequence,³⁴ which consists of two hard pulses of 6 and 2 μs at an RF field of 70 kHz, for triple-quantum excitation and reconversion, respectively, followed by a soft pulse of 14 μs at an RF field of 6 kHz. The t_1 step was set to the

MAS period. The HMQC experiments were set up with a ^{17}O spin echo selective to the central transition, with pulses of 10 and 20 μs . In the J-HMQC, the recoupling delay was set to 4 ms, with a ^1H π pulse of 2.25 μs . For the D-HMQC acquisition, the recoupling scheme (SR_4)³⁵ was applied for 1 ms. A total of 12800 transients were added with a recycling delay of 1.5 s. Chemical shifts were given in ppm with respect to TMS as external reference for ^1H NMR and to water for ^{17}O NMR.

Preparation of ^{17}O -Labeled Silica. Aerosil silica from Evonik (specific area of 200 $\text{m}^2 \text{g}^{-1}$) was treated at 1000 $^\circ\text{C}$ under high vacuum (10^{-5} Torr) for 15 h. Excess ^{17}O -enriched water (^{17}O content 70%) was introduced in the reactor and left to react at room temperature for 8 h. The material was then submitted to heat treatment under high vacuum (10^{-5} Torr) for 15 h at the desired temperature.

Theoretical Calculations. All DFT calculations were performed with Gaussian 03.³⁶ Calculations were carried out at the DFT level of theory using the hybrid functional B3PW91.³⁷ Geometry optimizations were achieved without any symmetry restriction. Calculations of vibrational frequencies were systematically done to characterize the nature of stationary points. Stuttgart effective core potentials and their associated basis set were used for silicon and tungsten.³⁸ The basis sets were augmented by a set of polarization functions ($\zeta_d = 0.284$ for Si and $\zeta_f = 0.823$ for W). Hydrogen, carbon, and oxygen atoms were treated with 6-31G(d,p) double- ζ basis sets.³⁹

The optimized structures were used for ^{17}O NMR calculations. These calculations were also performed using a higher Dunning's correlation consistent basis set cc-PVTZ for the oxygen atoms.⁴⁰ In all cases, among the various theories available to compute chemical shielding tensors, the Gauge Including Atomic Orbital (GIAO) method has been adopted for the numerous advantages it presents.⁴¹ Typically, to compare our calculations with experimental values, ^{17}O chemical shielding has been converted to chemical shift using the usual equation: $\delta_{\text{iso}} = \sigma_{\text{iso}}^{\text{ref}} - \sigma_{\text{iso}}^{\text{sample}}$, where $\sigma_{\text{iso}}^{\text{ref}}$ is the isotropic ^{17}O chemical shielding of the liquid water. However, because of the arbitrariness in the choice of the isotropic chemical shift of the reference—the value of $\sigma_{\text{iso}}^{\text{ref}}$ depends of the level of theory and the used basis sets⁴²—an internal reference is used for the calibration of the $\sigma_{\text{iso}}^{\text{ref}}$ value. As a consequence, we have calibrated the $\sigma_{\text{iso}}^{\text{ref}}$ value with respect to the ^{17}O CS of isolated silanol groups without interaction with organometallic fragments; that is, the calculated $\sigma_{\text{iso}}^{\text{sample}}$ of 287.6 ppm is attributed to an experimental CS of −7.4 ppm: $\sigma_{\text{iso}}^{\text{ref}} = 280.2$ ppm.

The ^{17}O quadrupolar coupling constant C_Q and the asymmetry parameter η_Q , which describes the interaction of the nuclear quadrupolar moment of the oxygen nuclei with the electric field gradient (EFG) arisen at these sites, are calculated from the EFG tensor eigenvalues V_{11} , V_{22} , and V_{33} following eqs 1 and 2:

$$C_Q \text{ (MHz)} = \frac{e^2 Q q}{h} = \frac{e Q V_{33}}{h} \quad (1)$$

$$\eta_Q = \frac{|V_{22}| - |V_{11}|}{|V_{33}|} \quad (2)$$

where Q is the nuclear quadrupole moment of the ^{17}O nucleus (in units of fm^2 , $1 \text{ fm}^2 = 0.01 \text{ barns}$) and $V_{33} = eq$, with the convention: $|V_{33}| \geq |V_{22}| \geq |V_{11}|$. The conversion from atomic units to MHz is as follows:

$$C_Q \text{ (MHz)} = -2.3496Q \text{ (fm}^2) V_{33} \text{ (au)} \quad (3)$$

The factor -2.3496 in eq 3 includes the natural constants and takes care of the units. Unfortunately, the published values of $Q(^{17}\text{O})$ often show large variations. The value of the ^{17}O nuclear quadrupole moment varies from -1.85 fm^2 to -2.6 fm^2 according to the level of theory.⁴³ It is therefore necessary to calibrate the value of Q . For this, we consider the same calibration methodology as that used by Dong et al.,^{43d} i.e., the comparison of the experimental and the theoretical values of the quadrupolar coupling constant of different small molecules for which accurate values of C_Q have been determined by high-resolution microwave spectroscopy. The DFT results are presented in Table S2 (Supporting Information). Combining the calculated EFGs and the experimental C_Q values, we obtained an effective $Q(^{17}\text{O})$ value of -2.3813 fm^2 .

■ ASSOCIATED CONTENT

📄 Supporting Information

Additional spectroscopic and DFT data and complete ref 36. This material is available free of charge via the Internet at <http://pubs.acs.org>.

■ AUTHOR INFORMATION

Corresponding Author

regis.gauvin@ensc-lille.fr; laurent.delevoeye@ensc-lille.fr; taoufik@cpe.fr; laurent.maron@irsamc.ups-tlse.fr

Notes

The authors declare no competing financial interest.

■ ACKNOWLEDGMENTS

We thank the CNRS, the French Ministry of Research and Higher Education, and the ANR (ANR-09-BLAN-0329-03, CADISCOM) for their generous support and the UCCS Directing Board for an internal grant. Financial support from the TGE RMN THC Fr3050 for conducting the research is gratefully acknowledged. Dr. Elise Berrier is thanked for fruitful discussions.

■ REFERENCES

- (1) Thomas, J. M.; Thomas, W. J. *Principles and practice of heterogeneous catalysis*; Wiley-VCH: Weinheim, 1997.
- (2) Niemantsverdriet, J. W. *Spectroscopy in Catalysis*, 2nd ed.; Wiley-VCH: Weinheim, 2000.
- (3) *Multinuclear solid-state NMR of inorganic materials*; MacKenzie, K. J. D., Smith, M. E., Eds.; Pergamon Materials Series; Elsevier: 2002; Vol. 6.
- (4) Blanc, F.; Copéret, C.; Lesage, A.; Emsley, L. *Chem. Soc. Rev.* **2008**, *37*, 518.
- (5) Frydman, L. In *Encyclopedia of Nuclear Magnetic Resonance*; Grant, D. M., Harris, R. K., Eds.; John Wiley & Sons: Chichester, 2002; Vol. 9, p 262.
- (6) Ashbrook, S. E.; Smith, M. E. *Chem. Soc. Rev.* **2006**, *35*, 718.
- (7) (a) Fontenot, C. J.; Wiench, J. W.; Schrader, G. L.; Pruski, M. J. *Am. Chem. Soc.* **2002**, *124*, 8435. (b) Peng, L.; Huo, H.; Gan, Z.; Grey, C. P. *Microporous Mesoporous Mater.* **2008**, *109*, 156.
- (8) Vansant, E. F., Van Der Voort, P., Vrancken, K. C. *Characterization and chemical modification of the silica surface*; Elsevier: New York, 1995.
- (9) Delattre, L.; Babonneau, F. *Chem. Mater.* **1997**, *9*, 2385.
- (10) Klug, C. A.; Kroeker, S.; Aguiar, P. M.; Zhou, M.; Stec, D. F.; Wachs, I. E. *Chem. Mater.* **2009**, *21*, 4127.

- (11) (a) Marks, T. J. *Acc. Chem. Res.* **1992**, *25*, 57. (b) Wegener, S. L.; Marks, T. J.; Stair, P. C. *Acc. Chem. Res.* **2012**, *45*, 206. (c) *Modern Surface Organometallic Chemistry*; Basset, J.-M., Psaro, R., Roberto, D., Ugo, R., Eds.; Wiley-VCH: Weinheim, 2009.
- (12) Flambard, A.; Montagne, L.; Delevoeye, L. *Chem. Commun.* **2006**, 3426–3428.
- (13) Bunker, B. C.; Haaland, D. M.; Michalske, T. A.; Smith, W. L. *Surf. Sci.* **1989**, *222*, 95.
- (14) (a) Bronnimann, C. E.; Zeigler, R. C.; Maciel, G. E. *J. Am. Chem. Soc.* **1988**, *110*, 2023. (b) Liu, C. C.; Maciel, G. E. *J. Am. Chem. Soc.* **1996**, *118*, 5103. (c) Hartmeyer, G.; Marichal, C.; Lebeau, B.; Rigolet, S.; Caultet, P.; Hernandez, J. *J. Phys. Chem. C* **2007**, *111*, 9066.
- (15) Walter, T. H.; Turner, G. L.; Oldfield, E. *J. Magn. Reson.* **1988**, *76*, 106–120.
- (16) (a) Massiot, D.; Fayon, F.; Alonso, B.; Trébosc, J.; Amoureux, J.-P. *J. Magn. Reson.* **2003**, *164*, 160. (b) Mazoyer, E.; Trébosc, J.; Baudouin, A.; Boyron, O.; Pelletier, J.; Basset, J.-M.; Vitorino, M. J.; Nicholas, C. P.; Gauvin, R. M.; Taoufik, M.; Delevoeye, L. *Angew. Chem., Int. Ed.* **2010**, *49*, 9854.
- (17) (a) Grandinetti, P. J.; Baltisberger, J. H.; Farnan, I.; Stebbins, J. F.; Werner, U.; Pines, A. *J. Phys. Chem.* **1995**, *99*, 12341. (b) Gervais, C.; Babonneau, F.; Smith, M. E. *J. Phys. Chem. B* **2001**, *105*, 1971.
- (18) Clark, T. M.; Grandinetti, P. J.; Florian, P.; Stebbins, J. F. *Phys. Rev. B* **2004**, *70*, 064202.
- (19) (a) Copéret, C.; Chabanas, M.; Petroff Saint-Arroman, R.; Basset, J.-M. *Angew. Chem., Int. Ed.* **2003**, *42*, 156. (b) Thomas, J. M.; Raja, R.; Lewis, D. W. *Angew. Chem., Int. Ed.* **2005**, *44*, 6456.
- (20) (a) Quignard, F.; Lecuyer, C.; Bougault, C.; Lefebvre, F.; Choplin, A.; Olivier, D.; Basset, J.-M. *Inorg. Chem.* **1992**, *31*, 928. (b) Lefort, L.; Chabanas, M.; Maury, O.; Meunier, D.; Copéret, C.; Thivolle-Cazat, J.; Basset, J.-M. *J. Organomet. Chem.* **2000**, *593–594*, 96. (c) Le Roux, E.; Taoufik, M.; Chabanas, M.; Alcor, D.; Baudouin, A.; Copéret, C.; Thivolle-Cazat, J.; Basset, J.-M.; Lesage, A.; Hediger, S.; Emsley, L. *Organometallics* **2005**, *24*, 4274.
- (21) Julian, B.; Gervais, C.; Rager, M.-N.; Maquet, J.; Cordocillo, E.; Escibano, P.; Babonneau, F.; Sanchez, C. *Chem. Mater.* **2004**, *16*, 521.
- (22) Gajan, D.; Copéret, C. *New J. Chem.* **2011**, *35*, 2403.
- (23) (a) Ajjou, J. A. N.; Scott, S. L.; Paquet, V. *J. Am. Chem. Soc.* **1998**, *120*, 415. (b) Ajjou, J. A. N.; Rice, G. L.; Scott, S. L. *J. Am. Chem. Soc.* **1998**, *120*, 13436.
- (24) Rioulet, V.; Taoufik, M.; Basset, J.-M.; Lefebvre, F. *J. Organomet. Chem.* **2007**, *692*, 4193.
- (25) Trébosc, J.; Hu, B.; Amoureux, J. P.; Gan, Z. *J. Magn. Reson.* **2007**, *186*, 220.
- (26) Le Roux, E.; Chabanas, M.; Baudouin, A.; de Mallmann, A.; Copéret, C.; Quadrelli, E. A.; Thivolle-Cazat, J.; Basset, J.-M.; Lukens, W.; Lesage, A.; Emsley, L.; Sunley, G. J. *J. Am. Chem. Soc.* **2004**, *126*, 13391.
- (27) Wolke, S. I.; Buffon, R. *J. Mol. Catal. A* **2000**, *160*, 181.
- (28) Joubert, J.; Delbecq, F.; Sautet, P.; Le Roux, E.; Taoufik, M.; Thieuleux, C.; Blanc, F.; Copéret, C.; Thivolle-Cazat, J.; Basset, J.-M. *J. Am. Chem. Soc.* **2006**, *128*, 9157.
- (29) (a) Del Rosal, I.; Gerber, I. C.; Poteau, R.; Maron, L. *J. Phys. Chem. A* **2010**, *114*, 6322. (b) Del Rosal, I.; Poteau, R.; Maron, L. *Dalton Trans.* **2011**, *40*, 11211. (c) Del Rosal, I.; Poteau, R.; Maron, L. *Dalton Trans.* **2011**, *40*, 11228.
- (30) See for instance, chapter 3, page 64 in ref 7.
- (31) Rhers, B.; Quadrelli, E. A.; Baudouin, A.; Taoufik, M.; Copéret, C.; Lefebvre, F.; Basset, J.-M.; Fenet, B.; Sinha, A.; Schrock, R. R. *J. Organomet. Chem.* **2006**, *691*, 5448.
- (32) Fleischman, S. D.; Scott, S. L. *J. Am. Chem. Soc.* **2011**, *133*, 4847.
- (33) Frydman, L.; Hardwood, J. *J. Am. Chem. Soc.* **1995**, *117*, 5367.
- (34) Amoureux, J.-P.; Fernandez, C.; Steuernagel, S. *J. Magn. Reson.* **1996**, *A123*, 116.
- (35) Brinkmann, A.; Kentgens, A. *J. Am. Chem. Soc.* **2006**, *128*, 14758.
- (36) Frisch, M. J.; et al. *Gaussian 03 (Revision B.05)*; 2003. See Supporting Information for complete reference.

- (37) (a) Perdew, J. P. In *Electronic structure of solids*; Ziesche, P., Eschrig, H., Eds.; Akademie: Berlin, 1991; Chapter Unified Theory of Exchange and Correlation Beyond the Local Density Approximation. (b) Perdew, J. P.; Burke, K.; Wang, Y. *Phys. Rev. B* **1996**, *54*, 16533. (c) Burke, K.; Perdew, J. P.; Wang, Y. In *Electronic density functional theory: recent progress and new directions*; Dobson, J. F., Vignale, G., Das, M. P., Eds.; Plenum: New York, 1997. (d) Perdew, J. P.; Chevary, J. A.; Vosko, S. H.; Jackson, K. A.; Pederson, M. R.; Singh, D. J.; Fiolhais, C. *Phys. Rev. B* **1992**, *46*, 6671. (e) Perdew, J. P.; Burke, K.; Wang, Y. *Phys. Rev. B* **1998**, *57*, 14999. (f) Perdew, J. P.; Chevary, J. A.; Vosko, S. H.; Jackson, K. A.; Pederson, M. R.; Singh, D. J.; Fiolhais, C. *Phys. Rev. B* **1993**, *48*, 4978.
- (38) Küchle, W.; Dolg, M.; Stoll, H.; Preuss, H. *Mol. Phys.* **1991**, *74*, 1245.
- (39) (a) Harihara, P. C.; Pople, J. A. *Theor. Chim. Acta* **1973**, *28*, 213. (b) Hehre, W. J.; Ditchfield, R.; Pople, J. A. *J. Chem. Phys.* **1972**, *56*, 2257.
- (40) (a) Davidson, E. R. *Chem. Phys.* **1996**, *260*, 514. (b) Woon, D. E.; Dunning, T. H. *J. Chem. Phys.* **1993**, *98*, 1358.
- (41) (a) Wolinski, K.; Hilton, J. F.; Pulay, P. *J. Am. Chem. Soc.* **1990**, *112*, 8251. (b) McWeeny, R. *Phys. Rev.* **1962**, *126*, 1028. (c) London, F. J. *Phys. Radium* **1937**, *8*, 397. (d) Dodds, J. L.; McWeeny, R.; Sadlej, A. J. *Mol. Phys.* **1980**, *41*, 1419. (e) Ditchfield, R. *Mol. Phys.* **1974**, *27*, 789. (f) Junk, P. C.; Steed, J. W. *J. Organomet. Chem.* **1999**, *587*, 191.
- (42) (a) Walishen, R. E.; Mooibroek, S.; Macdonald, J. B. *J. Chem. Phys.* **1984**, *81*, 1057. (b) Kongsted, J.; Nielsen, C. B.; Mikkelsen, K. V.; Christiansen, O.; Ruud, K. *J. Chem. Phys.* **2007**, *126*, 034510.
- (43) (a) Kamper, R. A.; Lea, K. R.; Lustig, C. D. *Proc. Phys. Soc. B* **1957**, *70*, 897. (b) Schaefer, H. F., III; Klemm, R. A.; Harris, F. E. *Phys. Rev.* **1969**, *181*, 137. (c) De Luca, G.; Russo, N.; Köster, A. M.; Calaminici, P.; Jug, K. *Mol. Phys.* **1999**, *97*, 347. (d) Dong, S.; Ida, R.; Wu, G. *J. Phys. Chem. A* **2000**, *104*, 11194. (e) Pyykkö, P. *Mol. Phys.* **2001**, *99*, 1617. (f) Larin, A. V.; Vercauteren, D. P. *Int. J. Quantum Chem.* **2001**, *82*, 182.